Binding Affinity of Metal Ions to the CD11b A-domain Is Regulated by Integrin Activation and Ligands*

Kaouther Ajroud‡§, Takashi Sugimori‡§, Wolfgang H. Goldmann‡§, Dahmani M. Fathallah¶, Jian-Ping Xiong‡, and M. Amin Arnaout‡‖

From the ‡Leukocyte Biology and Inflammation Program, Renal Unit, Massachusetts General Hospital and Harvard Medical School, Charlestown, Massachusetts 02129 and the ¶Molecular Biotechnology Group, Laboratory of Immunology, Institute Pasteur, 1002 Bélvédère, Tunis, Tunisia

The divalent cations Mg^{2+} and Ca^{2+} regulate the interaction of integrins with their cognate ligands, with Mg^{2+} uniformly facilitating and Ca^{2+} generally inhibiting such interactions *in vitro*. Because both cations are present in mM concentrations *in vivo*, the physiologic relevance of the *in vitro* observations is unclear. We measured the affinity of both cations to the inactive and active states of the ligand- and cation-binding A-domain (CD11bA) from integrin CD11b/CD18 in the absence and presence of the single-chain 107 antibody (scFv107), an activation-insensitive ligand-mimetic antibody. Using titration calorimetry, we found that Mg^{2+} and Ca^{2+} display equivalent (mM) affinities to inactive CD11bA. Activation induced a ~10-fold increase in the binding affinity of Mg^{2+} to CD11bA with no change in that of Ca^{2+} (106 μM ± 16 and 2.1 mM ± 0.19, respectively, $n = 4$). This increase is largely driven by favorable enthalpy. scFv107 induced a 50–80-fold increase in the binding affinity of Ca^{2+} (but not Mg^{2+} or Mn^{2+}) to either form of CD11bA. Thus the affinity of metal ions to integrins is itself regulated by the activation state of these receptors and by certain ligands. These findings, which we expect will be applicable *in vivo*, elucidate a new level of regulation of the integrin-metal-ligand ternary complex and help explain some of the discrepant effects of Ca^{2+} on integrin-ligand interactions.

Heterodimeric $\alpha\beta$ integrins are a large family of cell surface receptors that mediate cell-cell and cell-matrix adhesion, thus regulating most functions of living cells (1, 2). The divalent cation-dependent binding of physiologic ligands to integrins is triggered allosterically by "inside-out" activation signals that are propagated across the plasma membrane to induce ligand competency of the ectodomain. Liganded integrins in turn initiate signals that travel from "outside-in" to modify cell behavior. This bidirectional signaling is tightly regulated to ensure the proper titration of cell adhesion to physiologic needs.

Structural studies of integrins have elucidated the basis of metal-dependent ligand binding (3–6). Integrins contain a ligand-binding von Willebrand factor A-domain in the α- and/or β-subunits (αA[1] and βA, respectively). αA (or I-domain) assumes a nucleotide-binding (Rossmann) fold with a mostly parallel β-sheet surrounded by α-helices (Fig. 1). Ligand binding is mediated by a divalent cation at the apex of the β-sheet, which coordinates side chains from three non-contiguous surface loops. A glutamate residue from the ligand completes an octahedral coordination sphere around the metal (Fig. 1), with ligand binding specificity arising from additional contacts made with the surrounding surface of the integrin. The ligand-binding site in αA is named the metal ion-dependent adhesion site (MIDAS). Structural and biophysical studies as well as mutagenesis have revealed "open" and "closed" states of αA corresponding to active and inactive states, respectively (7–9). The open and closed states in the native integrin are in a dynamic equilibrium that normally favors the closed state in quiescent cells (10). The open state (*versus* closed) is characterized by a changed position and packing of the F-α7 loop (between the F strand and the C-terminal α7 helix), an inward movement of the α1 helix, and a 10-Å downward slide of the α7 helix (Fig. 1) (11). These tertiary changes alter metal ion coordination at MIDAS and the shape and charge of the MIDAS face, enabling it to bind physiologic ligands (5, 6). The active state is favored/stabilized by bound ligand (7). It can also be induced allosterically by destabilizing the hydrophobic contact of α7 with the central β-sheet (8, 10). This allosteric up-regulation can be produced *in vitro* by a Gly substitution of the invariant α7 residue Ile^{316}, which resides in the hydrophobic site-for-isoleucine (SILEN) pocket in inactive CD11bA (Fig. 1) (8, 9), or by engineered disulfides resulting in an open but unliganded conformation (12). In integrins with both αA- and βA-domains, a conserved C-terminal glutamate from open αA acts as an endogenous ligand by contacting the MIDAS cation in βA (13, 14). This allows the propagation of conformational changes from one domain to the other in the whole integrin, providing a basis for bidirectional signaling. The MIDAS face of liganded βA is decorated by two additional metal ions at ADMIDAS (adjacent to MIDAS) and at the ligand-associated metal-binding site (LIMBS) on either side of MIDAS (6). In unliganded βA, only ADMIDAS is occupied by a metal that links the α1 helix to the F-α7 loop, maintaining the integrin in a low affinity state. In the liganded state, a metal ion is bound at MIDAS with a ligand Asp completing its coordination sphere in a manner strikingly similar to that in αA. In the liganded state, the ADMIDAS metal ion shifts inwards toward MIDAS,

§ These authors contributed equally to this work.
‖ To whom correspondence should be addressed: Renal Unit, Massachusetts General Hospital, 149 13th St., Charlestown, MA 02129. Tel.: 617-726-5663; Fax: 617-726-5671; E-mail: arnaout@receptor.mgh.harvard.edu.
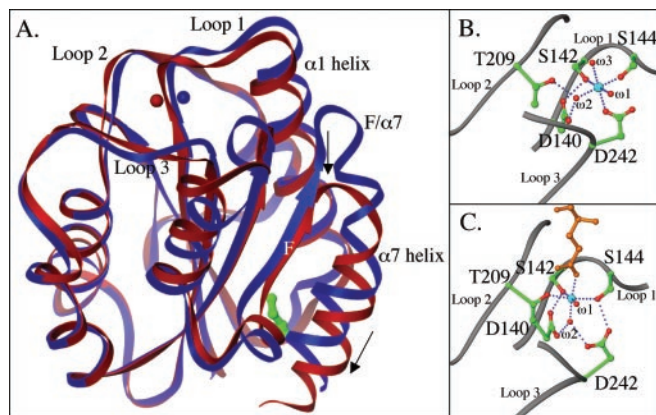
[1] The abbreviations used are: αA and βA, α- and β-subunits, respectively, of the ligand-binding von Willebrand factor A-domain of integrins; MIDAS, metal ion-dependent adhesion site; ADMIDAS, adjacent to MIDAS; mAb, monoclonal antibody; H-CDR3, heavy chain complementarity-determining region 3.

helping to stabilize the MIDAS cation, with the $\alpha 1$ helix moving in unison. The F-$\alpha 7$ loop undergoes a major conformational change, and its link with ADMIDAS is severed. A third metal ion occupies the ligand-associated metal-binding site, serving also to stabilize the MIDAS ion and therefore to ensure the stable binding of the ligand (6). As in the case of αA, the changes in βA can be ligand-induced or may be triggered allosterically through a conformational switch of the F-$\alpha 7$ loop driven directly by an inside-out signal as proposed in the dead bolt model (2).

It is established that the nature of the metal ion plays a critical role in regulating ligand binding affinity to αA (for review, see Ref. 15). In many αA-integrins, μM Mg^{2+} or Mn^{2+} (but not μM Ca^{2+}) supports ligand binding, and mM Ca^{2+} blocks Mg^{2+}-mediated adhesion (16–21). On the other hand, μM Ca^{2+} was found to support ligand binding to some αA-domains (21) and to the respective native integrins (22–24), an effect that can be mediated through a direct coordination of Ca^{2+} at MIDAS (21, 25). The reason(s) for the opposing effects of Ca^{2+} on ligand binding in αA-integrins is not well understood. Further,

since human plasma contains mM concentrations of Mg^{2+} and Ca^{2+}, the physiologic relevance of the above observations is currently unclear.

Despite extensive studies of the role of metal ions in integrin function, the possibility that metal ion binding to integrins is itself regulated by the activation state of the integrin has not been explored. One reason is that integrins contain multiple metal-binding sites, making such a determination in the native integrin difficult (6). Second, some physiologic ligands contain metal-binding sites of their own, complicating such an analysis (26, 27). Third, physiologic ligands bind integrins in an activation-dependent manner (1), making it difficult to evaluate an independent role of integrin activation on metal ion binding affinity *per se*. Forth, physiologic ligands form multivalent interactions with integrins, sometimes with distinct metal ion requirements; for example, the binding of integrin CD11a/CD18 to CD54 is Mg^{2+}-dependent, yet clustering of this integrin is Ca^{2+}-dependent (28). The feasibility of producing functionally and structurally defined water-soluble forms of αA (8, 9) and the availability of an activation-independent ligand-mimetic mAb 107 (29) allowed us to explore whether metal ion affinity is regulated by the activation state of αA and/or by the ligand. We found that although both Mg^{2+} and Ca^{2+} display low (mM) affinity to MIDAS in inactive αA from integrin CD11b/CD18 (CD11bA), Mg^{2+} selectively binds to MIDAS with μM affinity in the active state. The single-chain mAb 107 (scFv107) induced a dramatic increase in the affinity of MIDAS to Ca^{2+}, favoring it over Mg^{2+}. The significance of these findings is discussed below.
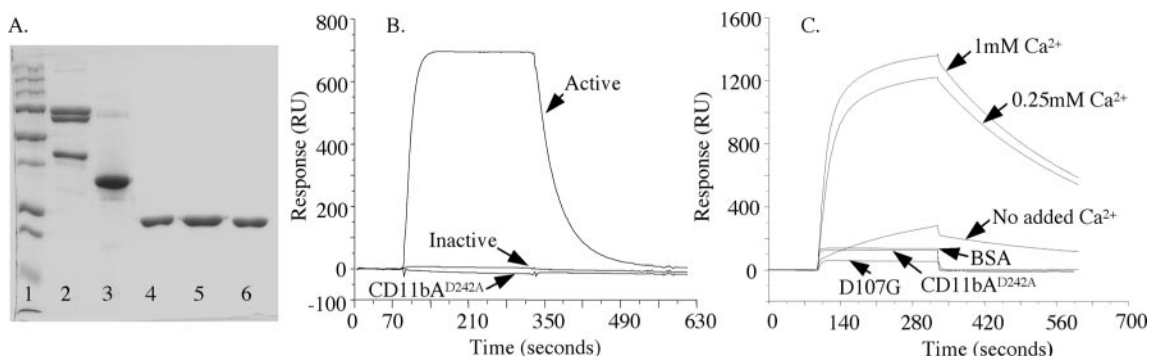
EXPERIMENTAL PROCEDURES

Protein Purification—The inactive form of CD11bA was generated by expressing a protein fragment spanning residues Gly^{123}–Gly^{321} ($CD11bA^{123-321}$) of human CD11b (8). The active form of CD11bA was made by replacing Ile^{316} with Gly ($CD11bA^{I316G}$) (8). The MIDAS-defective mutant $CD11bA^{D242A}$ has been described previously (3). All proteins were expressed as glutathione S-transferase fusion proteins in *Escherichia coli*, purified by affinity chromatography, cleaved with thrombin to release recombinant CD11bA, and further purified by ion exchange chromatography on a HiTrap SP Sepharose high performance column (Amersham Biosciences) using fast protein liquid chromatography (Amersham Biosciences). Purified preparations of CD11bA were dialyzed against 20 mM Tris-HCl, pH 7.5, 150 mM NaCl (Tris-buffered saline).

Expression and Purification of Single-chain 107—cDNAs encoding the variable heavy and kappa light chains of monoclonal antibody 107 were isolated by reverse transcription of mRNA derived from the 107 hybridoma cell line (29) using standard primers (30). A 93-bp DNA

FIG. 1. **Structural comparisons of closed and open CD11bA.** *A*, ribbon diagrams of the superimposed structures of closed (*blue*) and open (*red*) CD11bA. The MIDAS cation for each structure is indicated in the respective color. The invariant Ile^{316} is in *green* in the closed form but invisible in the open structure. The major conformational differences are indicated (see text for details). *B* and *C*, MIDAS cation (*cyan*) coordination in closed (*B*) and open (*C*) CD11bA by residues from three surface loops. Selected hydrogen bonds are shown as *blue dotted lines*. Amino acid side chains are in *green* with oxygen atoms in *red*. The backbone is in *gray*. The ligand glutamate is in *gold*. Water molecules are labeled $\omega 1$–$\omega 3$.

FIG. 2. **Analysis of recombinant proteins.** *A*, reduced SDS-PAGE (12%) analysis of purified iC3b (*lane 2*), wild-type scFv107 (*lane 3*), and inactive (*lane 4*), active (*lane 5*), and metal-defective ($CD11bA^{D242A}$) (*lane 6*) CD11bA. *Lane 1*, molecular mass markers in kDa (Bio-Rad 161-0373: 250, 150, 100, 75, 50, 37, 25, 20, 15, and 10 kDa). 3–5 μg were applied in each lane. *B*, sensorgrams recording the interaction of soluble active and inactive CD11bA and $CD11bA^{D242A}$ with the activation-dependent ligand iC3b (9,500 resonance units (*RU*), immobilized on the sensor chip) in the presence of 1 mM Mg^{2+} plus 1 mM Ca^{2+}. Background binding to the bovine serum albumin-coupled chip was subtracted. *C*, sensorgrams showing binding of soluble inactive CD11bA to the activation-independent ligand-mimetic scFv107 (3,743 resonance units immobilized on the sensor chip) in the presence of different calcium concentrations. Binding in the absence of added Ca^{2+} is also shown (*No added Ca^{2+}*). CD11bA-scFv107 interactions in 1 mM Ca^{2+} when $CD11bA^{D242A}$ or immobilized $scFv107^{D107G}$ (*D107G*, 4,036 resonance units) was used with the wild-type partner are indicated. Background binding to the bovine serum albumin (*BSA*)-coupled sensor chip in 1 mM Ca^{2+} is also shown.

fragment encoding the flexible linker peptide (Gly$_4$-Ser)$_3$ (Amersham Biosciences) was used to join the variable heavy and kappa light chain cDNAs, generating the cDNA encoding scFv107. The latter was cloned into pPICZαB (Invitrogen) with a thrombin cleavage site and a poly-histidine tag introduced at the C terminus. The construct was then fully sequenced. The BstXI-linearized vector was electroporated into yeast *Pichia pastoris* KM71H strain (Invitrogen), and Zeocin-resistant clones were selected. Detection of secreted scFv107 was done by Western blotting using anti-mouse Fab (Sigma). Large scale protein expression was done as follows. Yeast was grown at 30 °C in buffered glycerol complex medium (BMGY) with maximum aeration (250 rpm) until the culture reached an A_{600} between 2 and 6. To induce protein expression, cells were centrifuged (1,500–3,000 × g) for 10 min at room temperature and resuspended at one-tenth of the original culture volume in buffered methanol complex medium (BMMY) containing 5% casamino acids. To maintain induction, methanol was added to a final concentration of 1% every 24 h. The time course of protein expression was followed until 120 h. The culture was then centrifuged, and the supernatant was concentrated using Amicon concentrator (Millipore) and dialyzed against 50 mM sodium acetate, pH 5. Dialyzed scFv107 (lacking the His tag) was passed through a cation-exchange SP column using fast protein liquid chromatography (Amersham Biosciences) and eluted with 160–300 mM sodium chloride. Fractions were pooled, immediately dialyzed against 20 mM Tris-HCl, pH 8.2, and concentrated using Centricon (Millipore) to a final concentration of 1 mg/ml. A ligand-defective scFv107 mutant was generated by replacing the putative Asp^{107} ligand in the heavy chain complementarity-determining region 3 (H-CDR3) with Gly (scFv107^{D107G}).

Surface Plasmon Spectroscopy—Surface plasmon spectroscopy (BIAcore AB, Uppsala, Sweden) was used to measure the kinetic parameters (apparent association and dissociation rate constants, K_{on} and K_{off}, respectively) and the apparent equilibrium constants (K_d) of the binding of inactive and active CD11bA to the physiologic ligand iC3b or to scFv107. iC3b, purified as described previously (31), or scFv107 was covalently coupled via primary amine groups to the dextran matrix of a CM5 sensor chip (BIAcore). Chips treated in the same way using bovine serum albumin or no protein were used as negative controls. CD11bA (0.5 μM) was passed over the iC3b-, scFv-, or bovine serum albumin-coupled CM5 sensor chips or over bare CM5 sensor chips at 5 μl/min in Tris-buffered saline running buffer, pH 8.0, containing 0.005% P20, MgCl$_2$ + CaCl$_2$ (at 1 mM each), or various concentrations of CaCl$_2$ (0–1 mM). 1 M NaCl in 20 mM Tris-HCl, pH 8.0, or 10 mM HCl followed by 10 mM EDTA was used to remove the bound proteins on the chip and to regenerate the surface. The binding data (after subtracting the background binding to the bovine serum albumin-coupled surface) were analyzed by the linear transformation method to obtain the kinetic constants (32).

Titration Calorimetry—The heat flow resulting from the binding of metal ions to CD11bA, with or without ligand, was measured with high sensitivity isothermal titration calorimetry using a MicroCal VP-ITC microcalorimeter (MicroCal, Northampton, MA) with a reaction cell volume of V_{cell} = 1.4037 ml. CD11bA and scFv107 proteins were extensively dialyzed overnight at 4 °C in Tris-buffered saline. In a typical binding experiment, the calorimeter cell contained 0.1 mM CD11bA or scFv107 alone or a premixture of both (each at 0.1 mM) stirred at 260 rpm at 298 K (25 °C). In each case, the protein(s) was titrated with V_{inj} = 5–10 μl of a concentrated metal ion solution, which was injected 30 times at 2.5–5-min intervals. Each injection increased the total metal ion concentration in the calorimeter cell stepwise by δ_c = 6.2 μM. At the same time, the reaction volume was also increased, and a correction factor was applied for both reactant concentrations. For each titration, the corresponding control titrations were performed; *i.e.* the metal ion solution was injected into pure buffer (or pure buffer was injected into the protein solution), and the corresponding heats of dilution were subtracted from the heats measured for the binding reaction. All solutions were degassed immediately before use. The heats of protein dilutions were insignificant, so only the metal ion dilutions were used to correct total heats of binding prior to data analysis. The integrated heat effects were analyzed by nonlinear regression methods using the standard MicroCal ORIGIN software package 5. The experimental data were fitted to a model for simple binding to a single class of sites (n) on the protein. The enthalpy of binding, ΔH (kcal/degree/mol), was directly determined from the heat release, which is independent of the binding model. The association binding constant, K (M^{-1}), and the entropy, ΔS (cal − degree/mol), associated with each binding reaction were calculated from the standard expression $\Delta G = -RT \ln K = \Delta H - T\Delta S$. Values and uncertainties for n, K, and ΔH are weighted averages and weighted standard deviations from three or four titration
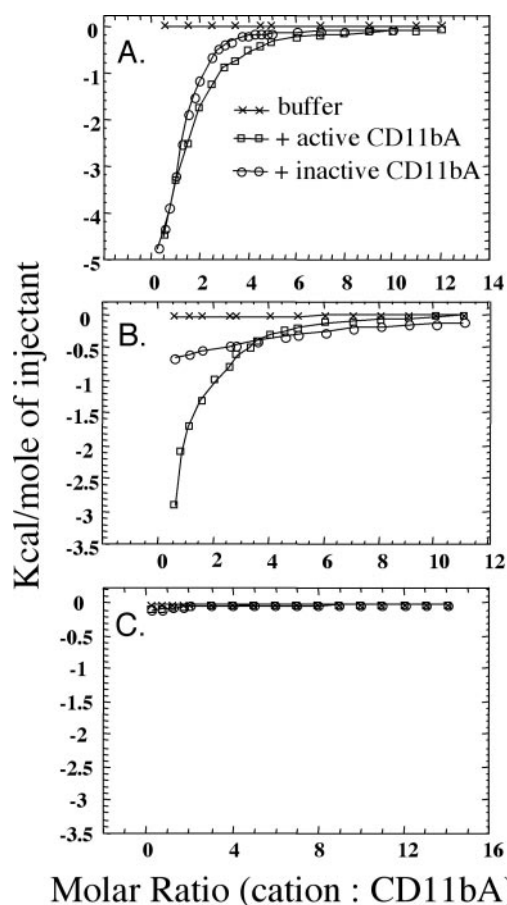

FIG. 3. **Affinity of divalent cations to inactive and active CD11bA.** Isothermal titration calorimetry of divalent cation binding to inactive and active CD11bA is shown. *A–C*, heats of reaction (kcal) derived from integration of the heat flow peaks/mol of the injected metal ion as a function of the molar ratio of the metal ion/CD11bA. The *solid lines* represent the least square fit to a single binding site model after subtracting the heat of dilution data (-×–×-). The integrated heat of binding of Mn^{2+} (*A*), Mg^{2+} (*B*), or Ca^{2+} (*C*) to inactive (○) and active (□) CD11bA at 298 K (25 °C) is shown.

runs, using the x^2 values and errors recovered from the fits. Values and uncertainties for the rest of the parameters were determined from these weighted average values and the propagation of their errors.

RESULTS

Characterization of CD11bA and scFv107 Recombinant Proteins—Gel electrophoresis of the purified inactive and active CD11bA, CD11bA^{D242A}, and scFv107 on SDS-containing reducing 12% polyacrylamide gels revealed single Coomassie Blue-stained bands of the expected molecular mass (Fig. 2*A*). Active but not inactive CD11bA bound to the physiologic ligand iC3b in Ca^{2+}- and Mg^{2+}-containing buffer as shown previously (8). As in the case of the native 107 mAb (29), Ca^{2+} alone mediated optimal binding of the activation-insensitive ligand-mimetic scFv107 to CD11bA (Fig. 2*C*). This binding required an intact MIDAS, as the CD11bA^{D242A} mutant, known to prevent metal ion coordination at MIDAS (3), abolished CD11bA-scFv107 interactions. Binding of scFv107 to inactive CD11bA required Asp^{107} in the H-CDR3 loop, as replacement of this residue with a glycine (D107G) markedly reduced the interaction (Fig. 1*C*).

Interaction of Mn^{2+} with Active and Inactive CD11bA—Use of titration calorimetry to measure affinity of metal ions to CD11bA was first established using Mn^{2+}, a metal ion that binds to the integrin with high affinity (3). A solution of inactive CD11bA (0.1 mM) in the calorimeter cell was titrated with a 0.65 mM solution of MnCl$_2$ at 25 °C. As the metal ion was

Affinity of Metal Ions to αA-Integrins Is Regulated

TABLE I
Dissociation constants for binding of divalent cations to the CD11b A-domains (mean ± S.D., n = 4 for "No ligand," n = 3 for "+scFv107")

Metal ion	Inactive				Active			
	K_d	$T\Delta S^0$	ΔH^0	ΔG^0	K_d	$T\Delta S^0$	ΔH^0	ΔG^0
	μM	*kcal/mol*			μM	*kcal/mol*		
No ligand								
Mn^{2+}	37 ± 6	0.17 ± 0.01	−5.87 ± 0.20	−6.04 ± 0.10	21 ± 7	−3.47 ± 0.53	−9.84 ± 0.86	−6.37 ± 0.21
Mg^{2+}	937 ± 88	3.48 ± 0.14	−0.65 ± 0.23	−4.13 ± 0.06	106 ± 16	−0.92 ± 0.23	−6.34 ± 0.38	−5.42 ± 0.09
Ca^{2+}	1900 ± 420	3.64 ± 0.10	−0.07 ± 0.06	−3.71 ± 0.13	2100 ± 190	3.62 ± 0.04	−0.03 ± 0.02	−3.65 ± 0.05
+scFv107								
Mn^{2+}	32 ± 5	−3.83 ± 0.24	−9.96 ± 0.39	−6.13 ± 0.06	21 ± 2	−5.28 ± 0.17	−11.65 ± 0.24	−6.37 ± 0.06
Mg^{2+}	1010 ± 101	3.48 ± 0.16	−0.60 ± 0.25	−4.08 ± 0.06	102 ± 15	1.09 ± 0.23	−4.34 ± 0.37	−5.44 ± 0.09
Ca^{2+}	40 ± 4	−0.80 ± 0.15	−6.79 ± 0.25	−5.99 ± 0.09	25 ± 3	−10.36 ± 0.19	−16.63 ± 0.30	−6.27 ± 0.07

added, heat was released, and as titration continued, the free protein concentration in the cell decreased. The heats of the reaction after integration of the titration peaks are shown in Fig. 3*A*; injection of the same metal ion solution into pure buffer had negligible heats of reaction. The ion-into-protein titration led to complete binding of CD11bA, with half-maximal heat amplitude obtained at Mn^{2+}/inactive CD11bA of ~1.0 (Fig. 3*A*), consistent with the presence of CD11bA in a monodisperse form and in agreement with the existing crystallographic data (11). The binding isotherm for the Mn^{2+}-inactive CD11bA interaction is characteristic of an exothermic single binding site interaction with μM binding affinity (37 ± 6, $n = 4$, Table I) and an observed enthalpy change (ΔH^0) of −5.87 ± 0.20 kcal/mol of Mn^{2+} (mean ± S.D., $n = 4$) (Table I). The standard free energy, $\Delta G^0 = -6.04 \pm 0.10$, is primarily enthalpy-driven and is accounted for by formation of new metal-protein bonds, with negligible contribution by a favorable temperature-dependent entropy ($T\Delta S^0 = 0.17 \pm 0.01$), resulting from the restricted movement of Mn^{2+} and CD11bA as they are joined together. The binding affinity of Mn^{2+} to active CD11bA proceeded with similar kinetics, with $\Delta G^0 = -6.37 \pm 0.21$, again driven primarily by favorable enthalpy ($\Delta H^0 = -9.84 \pm 0.86$) (Fig. 3*A* and Table I).

Interaction of Mg^{2+} with Inactive and Active CD11bA—In contrast to Mn^{2+}, the binding affinity of Mg^{2+} to the inactive and active forms of CD11bA was dramatically different. Binding to the former was of low affinity (0.937 ± 0.088 mM) (Fig. 3*B* and Table I), driven largely by favorable entropy (($T\Delta S^0 = 3.48 \pm 0.14$) with minimal contribution from enthalpy ($\Delta H^0 = -0.65 \pm 0.23$). With activation, the binding affinity of Mg^{2+} increased by ~10-fold ($K_d = 106 \pm 16$ μM), largely driven by favorable enthalpy ($\Delta H^0 = -6.34 \pm 0.38$) as with Mn^{2+} binding to active CD11bA. Half-maximal heat amplitude was obtained at a Mg^{2+}/active CD11bA of ~1.0, consistent with the presence of a single metal ion at MIDAS (4).

Interaction of Ca^{2+} with Active and Inactive CD11bA—We next assessed the binding affinity of Ca^{2+} to the two conformations of CD11bA. In both cases the binding affinity was very low (~2 mM) (Fig. 3*C* and Table I), largely driven by favorable entropy (Table I) as seen above with Mg^{2+} binding to inactive CD11bA.

Effect of Ligand on the Thermodynamics of Metal Ion-CD11bA Interactions—The binding affinity of the three metal ions to the inactive and active forms of CD11bA was next measured in the presence of scFv107. None of these metal ions bound to scFv107 directly in the absence of CD11bA (Fig. 4). Whereas the binding affinity of Mn^{2+} or Mg^{2+} to CD11bA did not change significantly, a 50-fold increase and an 80-fold increase in Ca^{2+} binding to inactive and active CD11bA, respectively, were observed (Fig. 4*C* and Table I). The binding energy for the Ca^{2+}-inactive CD11bA interaction is driven largely by favorable enthalpy; both favorable enthalpy and entropy contributed to Ca^{2+} binding to active CD11bA (Table I). In both
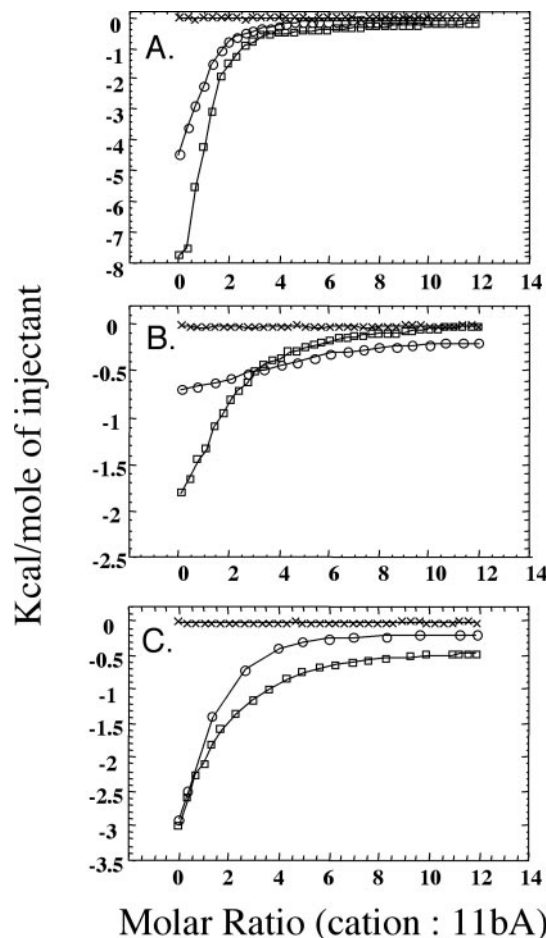

FIG. 4. **Role of the ligand in regulating affinity of divalent cations to CD11bA.** *A–C*, isothermal titration calorimetry of divalent cation binding to inactive and active CD11bA in the presence of scFv107. Integrated heat of binding of Mn^{2+} (*A*), Mg^{2+} (*B*), or Ca^{2+} (*C*) to inactive (○) and active (□) CD11bA at 298 K (25 °C) is shown. Data were fit to a single binding site model after subtracting the heat of dilution data as in Fig. 3. No metal binding was observed to scFv107 alone in *A–C* (-x–x-).

cases, half-maximal heat amplitude is obtained at a Ca^{2+}/CD11bA molar ratio of ~1.0, consistent with the presence of a single Ca^{2+}-binding site in CD11bA. This is most likely at MIDAS, as no binding of scFv107 to the MIDAS-defective mutant CD11bA^{D242A} occurs (Fig. 2*C*).

DISCUSSION

The major finding in this report is that the activation state as well as ligand regulate metal ion binding affinity to CD11bA. Activation induced a 10-fold increase in the binding affinity of Mg^{2+} but not Ca^{2+} to CD11bA. On the other hand, the ligand-mimetic scFv107 induced a dramatic increase in the binding

affinity of Ca^{2+} but not Mg^{2+} to CD11bA.

As shown previously, Mn^{2+} binds to inactive or active CD11bA with high (μM) affinity (3), and both Mn^{2+}-CD11bA interactions are dominated by favorable enthalpy. This high affinity is most likely accounted for by the known high electronegativity of this metal ion. The low binding affinity of Mg^{2+} to the inactive state and of Ca^{2+} to both the inactive and active states is largely driven by favorable entropy with little or a negligible contribution from enthalpy, consistent with their lower electronegativity. In this case, the favorable entropy could arise from electrostatic steering, which maximizes the frequency of productive encounters (33), from an increase in configurational entropy as a result of increased protein backbone or side chain mobility (34), or from release of solvent water from the metal-CD11bA binding interface (35), as the entropy of water increases as it leaves the protein surface to buffer. The single water molecule lost from MIDAS when CD11bA is liganded only contributes $\sim 0.69 \pm 0.48$ kcal/mol (36) to the favorable ΔG of the interaction (~ -4 kcal/mol), suggesting more important contributions from configurational entropy and electrostatic steering.

Whereas Mg^{2+} showed little binding to inactive CD11bA, it displayed a much higher affinity to the active state. The observed ~ 10-fold increase in affinity of Mg^{2+} to active CD11bA was driven largely by a favorable change in enthalpy and did not require binding of ligand (binding of scFv107 to CD11bA did not change Mg^{2+} affinity). These data indicate that integrin activation *per se* accounts for the dramatic increase in Mg^{2+} affinity to CD11bA. Coordination of the MIDAS metal ion is octahedral in both the closed and open states of CD11bA (4, 11). In the closed state, the bound metal ion is coordinated directly by the invariant hydroxyl oxygens of Ser^{142} and Ser^{144} from the conserved Asp-*X*-Ser-*X*-Ser motif (loop 1) and by the invariant carboxylate of Asp^{242} (loop 3) and is coordinated indirectly by the invariant Thr^{209} (loop 2) and Asp^{140} (loop 1) through two water molecules (Fig. 1). A third water molecule completes the metal coordination sphere. In the open "liganded" state, the hydroxyl oxygen of the Thr^{209} (loop 2) replaces Asp^{242} in directly coordinating the MIDAS metal ion, reducing its electrophilicity and facilitating a direct coordination of this metal by a glutamate from an exogenous ligand (Fig. 1). The present findings indicate that MIDAS displays a much higher affinity to Mg^{2+} in its open *versus* its closed configuration. This appears to be largely due to formation of a metal–protein bond (via the hydroxyl oxygen of Thr^{209}), which may account for the fact that the observed increase in affinity is largely enthalpy-driven (Table I).

In contrast to Mg^{2+}, the low (mM) affinity of Ca^{2+} to CD11bA was dramatically increased by ligand binding, with activation adding only slightly to the binding affinity. This increase was largely driven by a favorable change in enthalpy, which results from formation of a bond between the metal ion and the ligand Asp (Table I). mAb 107 binds to the MIDAS face of CD11bA in a metal-dependent but activation-independent manner (29), a characteristic of competitive protein antagonists of integrins such as NIF (neutrophil inhibitory factor) (29, 37) and mAb AQC2 (38), which inhibit CD11b/CD18 and $\alpha_1\beta_1$, respectively. In the case of mAb 107, this interaction requires an intact MIDAS and Asp^{107} from the H-CDR3 loop (Fig. 2*C*). A recently determined crystal structure of an αA from integrin $\alpha_1\beta_1$ in complex with mAb AQC2 in the presence of Mn^{2+} shows that an Asp from the H-CDR3 loop of the antibody coordinates the MIDAS ion directly as in the open state but without the downward movement of the C-terminal α7 helix (38). Modeling of the antigen-binding site of mAb 107 on that of the AQC2-integrin complex predicts that Asp^{107} from mAb 107 may act as a

MIDAS-coordinating ligand (not shown). Thus Asp^{107} from scFv107 may create a highly favored Ca^{2+} coordination site at MIDAS, accounting for the dramatic increase in binding affinity of Ca^{2+} to the closed CD11bA-scFv107 complex. It is also interesting to note that the critical influence of ligand on Ca^{2+} binding to MIDAS has also been observed in the βA-domain. In protein crystals of the αA-lacking integrin $\alpha_V\beta_3$, the βA MIDAS is metal-bound in the presence but not in the absence of the prototypical RGD ligand (5, 6). Also, in native $\alpha_4\beta_1$ (39) and $\alpha_9\beta_1$ (40), a rapidly exchangeable Ca^{2+}-binding site, presumably at MIDAS and of a similar affinity to that observed here for αA, is only detected in the presence of the ligand. Taken together, these data support the existence of a coupled equilibrium between ligand binding and MIDAS ion binding that is applicable to βA as well as to αA-domains in integrins.

Previous studies have shown that Mn^{2+} or Mg^{2+} but not Ca^{2+} supports binding of physiologic ligands to active CD11bA. In these cases, a ligand glutamate (rather than an aspartate) engages the MIDAS ion directly (7, 12). In view of the preferred Ca^{2+}-donor atom distances derived recently (41), we suggest that the longer glutamate side chain of physiologic ligands like iC3b and CD54 may prevent Ca^{2+} from forming a ternary ligand-metal-integrin complex. In the structure of the CD11aA-CD54-Mg^{2+} complex, for example, the extra 1.52-Å methyl group of the ligand glutamate might create a steric conflict for Ca^{2+} if it were to replace the MIDAS Mg^{2+} in this structure. In other instances where Ca^{2+} has been shown to support physiologic (glutamate-based) ligand binding (21), it is conceivable that the nature of the ligand binding interface allows an optimal coordination of Ca^{2+} at MIDAS. The present findings help explain several of the apparently discrepant effects of Ca^{2+} on αA-integrins. The present studies also reveal a potential activation-driven Ca^{2+}-Mg^{2+} exchange at MIDAS taking place under the physiologic mM concentrations of these cations, which may contribute to dynamic adhesion *in vivo*.

REFERENCES

1. Hynes, R. O. (2002) *Cell* **110,** 673–687
2. Xiong, J. P., Stehle, T., Goodman, S. L., and Arnaout, M. A. (2003) *Blood* **102,** 1155–1159
3. Michishita, M., Videm, V., and Arnaout, M. A. (1993) *Cell* **72,** 857–867
4. Lee, J. O., Rieu, P., Arnaout, M. A., and Liddington, R. (1995) *Cell* **80,** 631–638
5. Xiong, J. P., Stehle, T., Diefenbach, B., Zhang, R., Dunker, R., Scott, D. L., Joachimiak, A., Goodman, S. L., and Arnaout, M. A. (2001) *Science* **294,** 339–345
6. Xiong, J. P., Stehle, T., Zhang, R., Joachimiak, A., Frech, M., Goodman, S. L., and Arnaout, M. A. (2002) *Science* **296,** 151–155
7. Emsley, J., Knight, C. G., Farndale, R. W., Barnes, M. J., and Liddington, R. C. (2000) *Cell* **101,** 47–56
8. Xiong, J. P., Li, R., Essafi, M., Stehle, T., and Arnaout, M. A. (2000) *J. Biol. Chem.* **275,** 38762–38767
9. Vorup-Jensen, T., Ostermeier, C., Shimaoka, M., Hommel, U., and Springer, T. A. (2003) *Proc. Natl. Acad. Sci. U. S. A.* **100,** 1873–1878
10. Li, R., Rieu, P., Griffith, D. L., Scott, D., and Arnaout, M. A. (1998) *J. Cell Biol.* **143,** 1523–1534
11. Lee, J. O., Bankston, L. A., Arnaout, M. A., and Liddington, R. C. (1995) *Structure* **3,** 1333–1340
12. Shimaoka, M., Xiao, T., Liu, J. H., Yang, Y., Dong, Y., Jun, C. D., McCormack, A., Zhang, R., Joachimiak, A., Takagi, J., Wang, J. H., and Springer, T. A. (2003) *Cell* **112,** 99–111
13. Alonso, J. L., Essafi, M., Xiong, J. P., Stehle, T., and Arnaout, M. A. (2002) *Curr. Biol.* **12,** R340–R342
14. Yang, W., Shimaoka, M., Salas, A., Takagi, J., and Springer, T. A. (2004) *Proc. Natl. Acad. Sci. U. S. A.* **101,** 2906–2911
15. Leitinger, B., McDowall, A., Stanley, P., and Hogg, N. (2000) *Biochim. Biophys. Acta* **1498,** 91–98
16. Dransfield, I., Cabanas, C., Craig, A., and Hogg, N. (1992) *J. Cell Biol.* **116,** 219–226
17. Grzesiak, J. J., Davis, G. E., Kirchhofer, D., and Pierschbacher, M. D. (1992) *J. Cell Biol.* **117,** 1109–1117
18. Kern, A., Eble, J., Golbik, R., and Kuhn, K. (1993) *Eur. J. Biochem.* **215,** 151–159
19. Luque, A., Sanchez-Madrid, F., and Cabanas, C. (1994) *FEBS Lett.* **346,** 278–284
20. Mould, A. P., Akiyama, S. K., and Humphries, M. J. (1995) *J. Biol. Chem.* **270,** 26270–26277

21. Calderwood, D. A., Tuckwell, D. S., Eble, J., Kuhn, K., and Humphries, M. J. (1997) *J. Biol. Chem.* **272,** 12311–12317
22. Masumoto, A., and Hemler, M. E. (1993) *J. Cell Biol.* **123,** 245–253
23. Smith, J. W., Piotrowicz, R. S., and Mathis, D. (1994) *J. Biol. Chem.* **269,** 960–967
24. Onley, D. J., Knight, C. G., Tuckwell, D. S., Barnes, M. J., and Farndale, R. W. (2000) *J. Biol. Chem.* **275,** 24560–24564
25. Griggs, D. W., Schmidt, C. M., and Carron, C. P. (1998) *J. Biol. Chem.* **273,** 22113–22119
26. Doolittle, R. F., Spraggon, G., and Everse, S. J. (1998) *Curr. Opin. Struct. Biol.* **8,** 792–798
27. Guermonprez, P., Khelef, N., Blouin, E., Rieu, P., Ricciardi-Castagnoli, P., Guiso, N., Ladant, D., and Leclerc, C. (2001) *J. Exp. Med.* **193,** 1035–1044
28. van Kooyk, Y., Weder, P., Heije, K., and Figdor, C. G. (1994) *J. Cell Biol.* **124,** 1061–1070
29. Li, R., Haruta, I., Rieu, P., Sugimori, T., Xiong, J. P., and Arnaout, M. A. (2002) *J. Immunol.* **168,** 1219–1225
30. Orlandi, R., Gussow, D. H., Jones, P. T., and Winter, G. (1989) *Proc. Natl. Acad. Sci. U. S. A.* **86,** 3833–3837
31. Li, R., and Arnaout, M. A. (1999) *Methods Mol. Biol.* **129,** 105–124
32. Karlsson, R., Fagerstam, L., Nilshans, H., and Persson, B. (1993) *J. Immunol. Methods* **166,** 75–84
33. Janin, J. (1997) *Proteins* **28,** 153–161
34. Lee, K. H., Xie, D., Freire, E., and Amzel, L. M. (1994) *Proteins* **20,** 68–84
35. Brady, G. P., and Sharp, K. A. (1997) *Curr. Opin. Struct. Biol.* **7,** 215–221
36. Habermann, S. M., and Murphy, K. P. (1996) *Protein Sci.* **5,** 1229–1239
37. Rieu, P., Ueda, T., Haruta, I., Sharma, C. P., and Arnaout, M. A. (1994) *J. Cell Biol.* **127,** 2081–2091
38. Karpusas, M., Ferrant, J., Weinreb, P. H., Carmillo, A., Taylor, F. R., and Garber, E. A. (2003) *J. Mol. Biol.* **327,** 1031–1041
39. Chen, L. L., Whitty, A., Scott, D., Lee, W. C., Cornebise, M., Adams, S. P., Petter, R. C., Lobb, R. R., and Pepinsky, R. B. (2001) *J. Biol. Chem.* **276,** 36520–36529
40. Pepinsky, R. B., Mumford, R. A., Chen, L. L., Leone, D., Amo, S. E., Riper, G. V., Whitty, A., Dolinski, B., Lobb, R. R., Dean, D. C., Chang, L. L., Raab, C. E., Si, Q., Hagmann, W. K., and Lingham, R. B. (2002) *Biochemistry* **41,** 7125–7141
41. Harding, M. M. (2001) *Acta Crystallogr. Sect. D Biol. Crystallogr.* **57,** 401–411